










# Liquidhope: methylome and genomic profiling from very limited quantities of plasma-derived DNA

Eva María Trinidad , Enrique Vidal , Esther Coronado , Anna Esteve-Codina , Victoria Castell , Adela Cañete ,  
Marta Gut , Simon Heath <sup>†</sup> and Jaime Font de Mora <sup>†</sup>

Corresponding author. Eva M. Trinidad, Laboratory of Cellular and Molecular Biology and Clinical and Translational Research in Cancer, Health Research Institute Hospital La Fe, Avenida Fernando Abril Martorell, 106; Torre A, 5-0746026 Valencia, Spain. Tel.: +34-961246646; Fax: +34-963496620; E-mail: [eva\\_trinidad@iislafe.es](mailto:eva_trinidad@iislafe.es)

<sup>†</sup>Simon Heath and Jaime Font de Mora are joint senior authors.

## Abstract

Analysis of the methylome of tumor cell-free deoxyribonucleic acid (DNA; cfDNA) has emerged as a powerful non-invasive technique for cancer subtyping and prognosis. However, its application is frequently hampered by the quality and total cfDNA yield. Here, we demonstrate the feasibility of very low-input cfDNA for whole-methylome and copy-number profiling studies using enzymatic conversion of unmethylated cytosines [enzymatic methyl-seq (EM-seq)] to better preserve DNA integrity. We created a model for predicting genomic subtyping and prognosis with high accuracy. We validated our tool by comparing whole-genome CpG sequencing with *in situ* cohorts generated with bisulfite conversion and array hybridization, demonstrating that, despite the different techniques and sample origins, information on cfDNA methylation is comparable with *in situ* cohorts. Our findings support use of liquid biopsy followed by EM-seq to assess methylome of cancer patients, enabling validation in external cohorts. This advance is particularly relevant for rare cancers like neuroblastomas where liquid-biopsy volume is restricted by ethical regulations in pediatric patients.

**Keywords:** neuroblastoma, liquid biopsy, high-risk, MYCN, 11q, DNA methylation, combined haploinsufficiency

## Introduction

Tumor cell-free deoxyribonucleic acid (DNA; cfDNA) in the bloodstream holds valuable information about tumor genetics and epigenetics specific to each patient. Thus, liquid biopsy is rapidly becoming a relevant non-invasive method for cancer detection and monitoring of the disease. A major challenge today remains the limited amount of DNA that can be obtained from certain liquid biopsies in particular clinical settings [1]. Certainly, this is the case for pediatric tumors such as neuroblastoma where ethical considerations limit the amount and frequency of blood sample that can be taken from these young patients. Similarly, patients

with early stage cancer or patients in very poor general health are also not candidates for extraction of a large blood sample. Reduced representation bisulfite sequencing is one technique recently published which may be appropriate for small amounts of tumor-circulating DNA derived from liquid biopsies. Methylome profiling by reduced representation bisulfite sequencing enables the use of limited quantities of DNA, has an affordable cost and is an unbiased method. However, it covers less than 10% of the total CpG islands in the genome and only 60% of the promoter regions, significant limitations for precision medicine approaches. Additionally, this method excludes genes with none or distant

**Eva María Trinidad** is a postdoctoral researcher at Cellular and Molecular Biology lab and at Translational Research in Cancer Group in Health Research Institute Hospital La Fe (IISLaFe) in Valencia, Spain. Her research activity focuses on the field of cancer, immunology and immunotherapy.

**Enrique Vidal** is a Miguel Servet investigator with expertise in cancer bioinformatics who forms part of the Translational Research in Cancer Group in IISLaFe, Valencia, Spain. His research interests include bioinformatics, computational techniques and data analysis.

**Esther Coronado** is a PhD student at Cellular and Molecular Biology lab and at Translational Research in Cancer Group in IISLaFe, Valencia, Spain. Her research interests include the molecular aspects of pediatric cancer as neuroblastoma and osteosarcoma.

**Anna Esteve-Codina** is a postdoctoral researcher at National Center for Genomic Regulation (CNAG-CRG), Barcelona Institute of Science and Technology (BIST), Universitat Pompeu Fabra (UPF), Barcelona, Spain. Her research interests include bioinformatics and novel method for stratification to cancer diseases.

**Victoria Castell** is a pediatric oncologist at Pediatric Oncology Unit, La Fe University Hospital, Valencia, Spain and at Translational Research in Cancer Group in Health Research Institute Hospital La Fe (IISLaFe) in Valencia, Spain.

**Adela Cañete** is the current head at Pediatric Oncology Unit, La Fe University Hospital, Valencia, Spain. She is a researcher at Translational Research in Cancer Group in IISLaFe in Valencia, Spain, and a professor in School of Medicine, University of Valencia. She is also coordinates several clinical trials related with neuroblastoma.

**Marta Gut** is head of the Sequencing Unit at CNAG-CRG, BIST, UPF, Barcelona, Spain. Her research interests include bioinformatics, computational techniques and data analysis.

**Simon Heath** leads the Bioinformatics Development and Statistical Genomics team and is the Manager of the Functional Genomics unit at CNAG-CRG, BIST, UPF, Barcelona, Spain. His research interests include bioinformatics, novel stratification tool and data analysis.

**Jaime Font de Mora** is head of Cellular and Molecular Biology lab and at Translational Research in Cancer Group in IISLaFe, Valencia, Spain. He directs this consortium. His research interests concern the characterization of genes, signaling pathways and cellular mechanisms associated with the ontogeny, and pathogenesis of neuroblastoma and other cancer pediatric malignancies.

**Received:** August 3, 2022. **Revised:** November 4, 2022. **Accepted:** November 25, 2022

© The Author(s) 2023. Published by Oxford University Press.

This is an Open Access article distributed under the terms of the Creative Commons Attribution Non-Commercial License (<http://creativecommons.org/licenses/by-nc/4.0/>), which permits non-commercial re-use, distribution, and reproduction in any medium, provided the original work is properly cited. For commercial re-use, please contact [journals.permissions@oup.com](mailto:journals.permissions@oup.com)

CCGG motifs [2]. On the other hand, array-based methylated CpGs require vast amounts of DNA (over 150 ng) that are not committed in liquid biopsy samples.

Neuroblastoma is the most common extracranial solid tumor in infants and children and the high-risk is highly associated with relapse and death [3, 4]. Thus, high-risk neuroblastomas still require all our efforts to identify more efficient therapies and validated approaches to monitor the disease. Genetically, high-risk neuroblastomas are characterized by either *MYCN* amplification or lengthening of telomeres by *TERT* or by alternative mechanisms (*TERT/ALT*) [5–7]. In the *TERT/ALT* group, deletion of the long arm of chromosome 11 is a distinct subgroup because it has a similar poor outcome as *MYCN* amplification but they rarely coincide (1.4%) [8], suggesting that they are both independent genetic drivers of the disease. In high-risk neuroblastomas, 11q deletion correlates with the highest number of segmental chromosomal aberrations (SCA), indicating defects in DNA repair machinery. In contrast, 11q deletion may also occur with less frequency in the low-risk subgroup, but with few to none concomitant chromosome imbalances [9]. These results suggest that low- and high-risk neuroblastomas with 11q deletion have distinct phenotype and outcome, and that 11q deletion requires additional alterations (such as *TERT/ALT* and/or others) to change risk stratification. Other SCAs include gain of 2p and 17q, and loss of 1p, 3p and 4p, all considered frequent alterations in neuroblastoma [10, 11]. Neither *MYCN* amplification nor 11q deletion are currently directly actionable targets. However, evidences support the effective use of bromodomain inhibitors to target upstream transcription of *MYCN* in *MYCN*-amplified neuroblastomas, and *PARP* inhibitors to target DNA repair deficiency in 11q-deleted neuroblastomas, although sensitivity to drugs is conditioned to the lack of mutations in *PIK3CA* pathway and in *TP53*, respectively [8, 12–14].

DNA methylation is a major epigenetic mechanism, and numerous studies in neuroblastoma have associated promoter methylation levels in proapoptotic genes *CASP8*, *DCR1*, *DCR2* and *TMS1* with their expression levels [15–17]. *RASSF1A* promoter hypermethylation has been studied in different tumor types, and in neuroblastoma it has also been associated with poor outcome [18]. A more recent study with cfDNA showed its value as a molecular tumor marker [19]. Three different studies across neuroblastoma risk groups have reported differential methylation profiles of genes that are associated to prognosis (*SCNN1A*, *PRKCDBP*, *KRT19*; *HIST1H3C*, *GNAS* and a 58 gene signature) [20–22].

In order to expand our knowledge on the contribution of DNA methylation, focused solely on the high-risk neuroblastoma, we performed a genome-wide DNA methylation analyses in blood-derived cfDNA in a cohort of 64 patients at diagnosis (Liquidhope). We validated our results with two independent *in situ* DNA cohorts (Target and Westermann). Our results demonstrate that, regardless of the different biological sources, methodologies in 5-methylcytosine conversion and sequencing or arrays analysis, liquid biopsy cfDNA is an outstanding tool that faithfully represents the epigenomics signature of the tumor.

Altogether, our results reveal two prognostic actionable targets in high-risk 11q-deleted neuroblastomas and a robust DNA-methylation biomarker profile for accurate stratification of patients with high-risk neuroblastomas that could be used for monitoring the disease as well as for future clinical studies setting the targets toward *MYCN* amplification or 11q deletion (i.e. *BET* inhibitors or *PARP* inhibitors).

## Methods

### Patients and samples

A retrospective study was performed in a primary cohort of 64 patients diagnosed with primary high-risk neuroblastoma who underwent treatment between 2007 and 2019. These cases were collected from the archives of Hospital La Fe in Valencia. Clinical characteristics for each patient are summarized in [Supplementary Table S1](#). Around 1 ml of blood-derived plasma obtained at diagnosis was used to isolate cfDNA with the QIAamp circulating nucleic acids kit (QIAGEN). In addition, there was also available blood-derived plasma from 20 out of the 64 patients at relapse and isolated cfDNA from these samples was also analyzed. Quantity and quality of isolated cfDNA was determined by electrophoresis in Agilent 2200 TapeStation. The study was conducted in accordance with the reporting recommendations for tumor marker prognostic studies (REMARK), the Declaration of Helsinki and La Fe Research Ethics Committee approved this project, reference number 2018-02-09. Parents or legal guardians signed an informed consent statement for sample and data management.

### Enzymatic methyl-seq (EM-seq)

To prepare libraries for comprehensive methylome representation within a cfDNA, we used the NEBNext EM-seq (New England Biolabs, NEB), following the manufacturer's recommendations with minor modification that the cfDNA was not sheared. The method utilizes 10 ng starting material of cfDNA and relies on two step conversion of the cytosines. The first step uses TET2 oxidation of 5-methylcytosine that provides protection to the modified cytosines from conversion by APOBEC deamination, so only cytosines but not 5-methylcytosines are converted to uracil. Ultimately, cytosines are sequenced as thymines and 5-methylcytosines are sequenced as cytosines. The final 8 cycles of PCR library amplification were carried out using the NEB Unique dual index primer pairs (NEBNext multiplex oligos for Illumina).

The libraries were sequenced on NovaSeq 6000 (Illumina) in paired end with a read length of  $2 \times 151$  bp according to the manufacturer's protocol for dual indexing. Image analysis, base calling and quality scoring of the run are processed using the manufacturer's software Real Time Analysis (RTA 3.3.3) and followed by generation of FASTQ sequence files. A comprehensive quality assessment of the methylome generated from this technique is presented for each sample in [Supplementary Table S2](#).

### Data analysis of EM-seq

The EM-seq reads were processed using the gemBS pipeline v4.03 using as reference GRCh38 [23]. Reads with MAPQ scores  $< 20$  and read pairs mapping to the same start and end points on the genome were filtered out after the alignment step. The first five bases from each read were trimmed before the variant and methylation calling step to avoid artifacts due to end repair. For each sample, CpG sites were selected where both bases were called with a Phred score of at least 20, corresponding to an estimated genotype error level of  $\leq 1\%$ , and where the total number of reads informative for methylation from both strands combined was  $\geq 6$ . Sites with  $> 500x$  coverage depth were excluded to avoid centromeric/telomeric repetitive regions. Estimates of copy number were made from the sequencing depth using the computational tool *lb\_predict\_cn* from the package *lbtools* (v0.3.0) developed at the CNAG. *lbtools* contains a set of utilities for processing copy number estimates from whole genome liquid biopsy experiments. The source code and documentation for the

lbttools framework are available at <https://github.com/heathsc/lbttools/>. The copy number prediction was performed in bins of 10 kb, with each bin being corrected for GC content. The copy number estimates were also used to test for commonly observed structural variants found in neuroblastoma (MYCN expansion, 11q deletion, 1p deletion and 17q duplication). Testing was performed using the program `lb_region_test`, also available in the lbttools package, and used healthy samples from the Blueprint project as controls. For each tested region, robust estimates of the mean and SD of estimated copy number were made from the control samples. A t-test was then used to test for differences between each liquid biopsy sample and the control samples. In addition, for the 11q, 1p and 17q regions, an estimate of ctDNA fraction [24] was made assuming a single copy deletion in 11q or 1p, and a 2-copy duplication of 17q. The results of the copy number testing and ctDNA prediction for all 84 samples can be found in [Supplementary Table S3](#).

### MYCN/11q prediction modeling

The predictive model for mutation type MYCN amplification/11q deletion was an elastic net regression model generated using the package `glmnet` (v4.1-1) in R (v4.1). A set of 235 999 CpGs were selected for the model generation. Each CpG in the selected set passed the individual sample QC filters (described above) on at least 90% of the samples and, in addition, was in the set of CpGs covered by the Illumina Infinium Human Methylation 450 k array. In this way the generated model could also be applied to datasets generated from the 450 k array. The elastic net model was generated using the set of samples taken at diagnosis from the Liquidhope cohort that passed QC, where the sample had been classified as having either 11q deletion or MYCN amplification. The model was then applied exclusively to the high-risk patients in Target cohort, generating prediction of the mutation class for the subset of samples that were classified as being high-risk and, as for the Liquidhope cohort, had either a deletion of 11q or an amplification of MYCN. The novel script used to fit the model and test against the Target cohort is provided in [Supplementary File S1](#). For class prediction, we employed a logistic regression model using the `tidymodels` R library with 10-fold cross-validation and selecting `lambda` with highest ROC/AUC metric. For training, new examples of the under-represented class were generated using nearest neighbors with the `'step_smote'` function of the `themis` R package.

Target cohort containing bisulfite CpG conversion data was retrieved from [https://target-data.nci.nih.gov/Public/NBL/methylation\\_array/L3/](https://target-data.nci.nih.gov/Public/NBL/methylation_array/L3/). Similarly, the model was additionally validated in the high-risk patients of the Westermann cohort (R2 Genomics, <https://r2.amc.nl>) harboring either MYCN amplification or 11q deletion alone. For comparisons with the DNA methylation landscape of human early embryos, we also included available whole genome bisulfite sequencing data of human oocytes, sperm and blastocysts [25] as well as data from adrenal gland [26]. Processed methylation data were downloaded from <https://humandbs.biosciencedbc.jp/en/hum0009v1#hum0009v1.CpG.v1> and from <https://www.ncbi.nlm.nih.gov/geo/query/acc.cgi?acc=gse54719>. Blueprint samples' data [27] are available at <http://www.blueprint-genome.eu>.

### Expression analysis

The expression analysis of 52 selected CpGs and *RASSF1A* was evaluated thanks to R2: Genomics Analysis and Visualization Platform in Target cohort. We chose the high-risk patients in the `ensh37e59c` platform and assess only the expression of the 11q

deletion and MYCN amplification. In addition, mRNA-seq expressions were retrieved from <https://target-data.nci.nih.gov/Public/NBL/mRNA-seq/L3/expression/NCI-Khan/> for *ATM*, *ATR*, *BRCA1*, *BRCA2*, *CHEK1*, *CHEK2*, *H2AFX*, *MDC1*, *MRE11A*, *MYCN*, *PRKDC* and *RAD50* genes. Only high-risk patients and primary solid tumors were selected. This dataset consisted of 58 patients with 11q deletion (without MYCN amplification) and 25 patients with MYCN amplification (without 11q deletion).

## Results

### Liquidhope cohort validation

To identify epigenetic biomarkers that better stratify high-risk neuroblastomas and define tumor origin and etiology, we conducted a multivariate regression analysis of methylated cfDNA in a cohort of 64 primary high-risk neuroblastoma patients (see [Supplementary Table S1](#) for clinical variables). DNA samples were subjected to conversion of unmethylated cytosines followed by WGS, and data were first analyzed for copy number variations and epigenetic signatures in comparison with controls, and selected samples containing validated and contrasted tumor DNA were further compared to high-risk neuroblastomas in two external independent cohorts, Target and Westermann (see scheme in [Figure 1A](#)).

Our initial analysis to discriminate tumor from non-tumor cfDNA was based on Principal Components Analysis (PCA) of the 84 sequenced samples and 80 healthy control samples from a range of hematopoietic cell types from the Blueprint project (green circles, [Figure 1B](#)). The PCA was performed on the correlation matrix between the CpG methylation values of pairs of samples taken across all selected CpGs (CpG selection carried out as previously described in the methods section for MYCN/11q prediction modeling). This broad epigenetic analysis revealed that 13 samples clustered together with the non-tumor controls, suggesting that tumor DNA in them was absent or masked by non-tumor DNA that got probably released by blood cells during sample manipulation (yellow diamonds, [Figure 1B](#)). Moreover, none of these samples showed chromosomal copy number variations as the others did ([Figure 1C](#)). Most of the copy number variations identified in the tumor DNA samples were already expected, as previously determined in tumor samples at diagnosis by FISH for MYCN amplification and by MLPA or SNP arrays for 11q deletion. These results indicate that only 60 samples at diagnosis and 11 at relapse contained tumor cfDNA. Hence, we decided to focus our subsequent studies on diagnosis with the 60 samples that undoubtedly contained tumor DNA. Interestingly, we noted that PCA clearly separated samples containing 11q deletion from those with MYCN amplification (blue circles versus red squares, [Figure 1B](#)), suggesting that 11q deletion has distinct epigenetic signatures from MYCN amplification and thus, support different epigenetic origin. One case with both 11q deletion and MYCN amplification displayed epigenetic similarities to MYCN-amplified (black triangle, [Figure 1B](#)), perhaps because MYCN is a potent transcriptional factor that directly recruits and orchestrates epigenetic modifiers, diluting and blurring 11q-deleted signature. Six cases with neither MYCN amplification nor 11q deletion had a trend to be in between (light blue triangles, [Figure 1B](#)).

A total of 53 samples with only MYCN or 11q alterations were subsequently used in comparison studies with external cohorts. To make comparisons possible, we selected CpGs from our WGS Liquidhope cohort that were contained in the 450 K arrays from Illumina (see Materials and Methods), a technique used by both external cohorts.

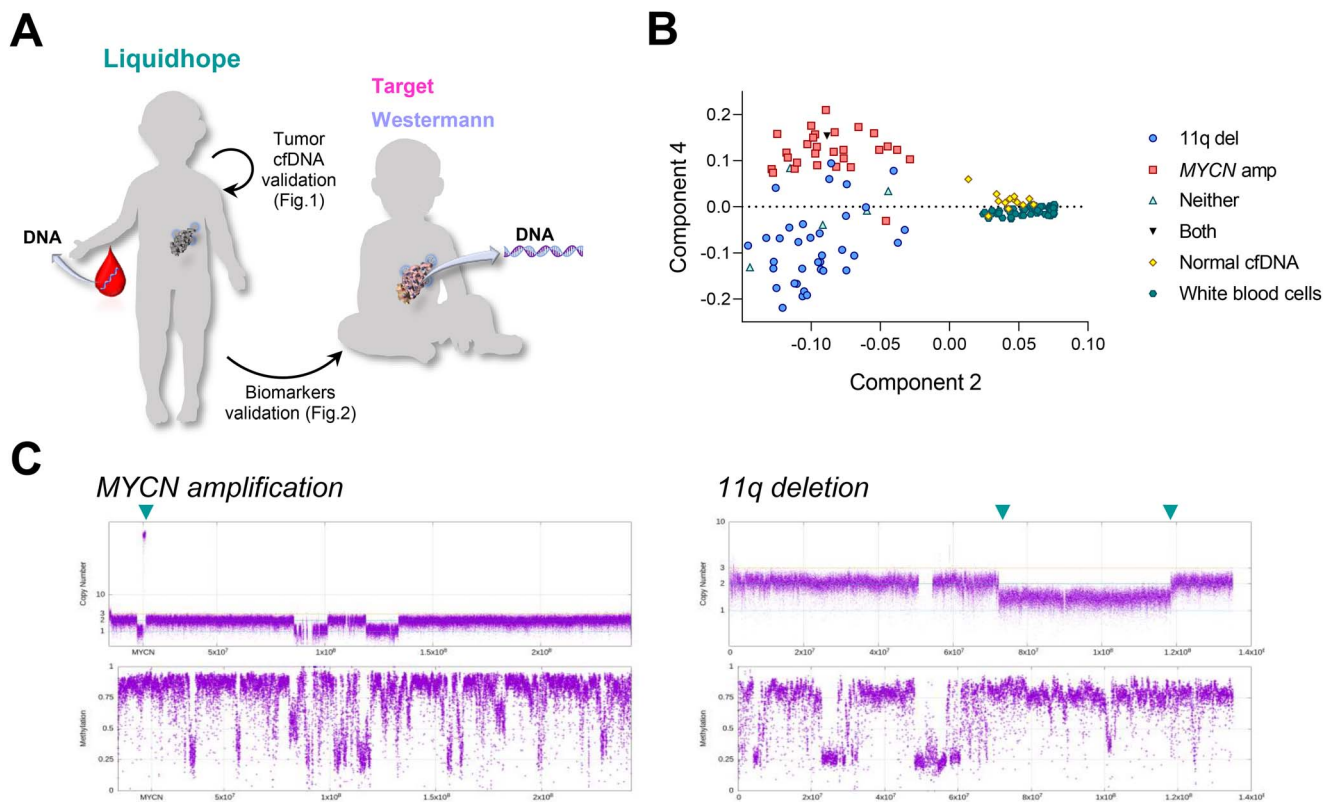


**Figure 1.** Isolated tumor cell-free circulating DNA (cfDNA) from liquid biopsy (blood-derived plasma) in neuroblastoma patients has the same genetic and epigenetic reliability as tumor biopsy. **(A)** Schematic overview illustrating self-validation in the Liquidhope cohort to ensure tumor DNA in each sample, and subsequent validation with high-risk neuroblastomas in Target cohort and in Westermann cohort. **(B)** Principal components model that discriminates MYCN amplification (MYCN amp), 11q deletion (11q del) and Liquidhope samples with undetectable tumor cfDNA (normal cfDNA) that cluster together with reference DNA from white blood cells. **(C)** Copy number variations (top graphs) and methylation profiles (bottom graphs) in two samples from Liquidhope cohort. Left panels correspond to whole chromosome 2 with MYCN amplification indicated by an arrow. Right panels correspond to chromosome 11 with the deleted segment flanked by two arrows.

We first compared the median methylation for each CpG between Liquidhope cohort and Target cohort. Only high-risk patients with either 11q deletion or MYCN amplification were used in the Target cohort. The results derived from this comparison showed a linear distribution of the data, demonstrating that both cohorts are rather comparable (Figure 2A). To further demonstrate that methylated CpG differences between 11q-deleted and MYCN-amplified neuroblastomas in our cohort are similar and comparable to the Target cohort, we conducted a comparison between both cohorts representing for each CpG the differences of median methylations between 11q-deleted minus MYCN-amplified tumors, resulting again in a linear distribution of the data (Supplementary Figure S1A). In contrast, comparison between both cohorts of median CpG methylations of patients that will not relapse minus those that will relapse resulted in a non-linear distribution (Supplementary Figure S1B). These results suggest that biomarkers of prognosis are not shared between cohorts but strongly support our subsequent comparisons to identify epigenetic signatures in 11q-deleted and MYCN-amplified tumors.

We next estimated ctDNA fraction for each sample, considering unbalanced chromosomes in 1p and 11q (expected changes from 2 copies to 1), and 17q (gaining from 2 copies to 3). In addition, we calculated MYCN CNVs and when amplified ( $\geq 10$ ), we defined sample as valuable tumor DNA content, especially in one case (AS2831) that did not display any of the above alterations (Supplementary Table S3).

We have also analyzed the linear distribution of the median CpG methylation in our Liquidhope cohort, comparing samples with ctDNA content (SCA content, including MYCN amplification or 11q deletion) versus the 13 samples that clustered together with normal DNA (Figure 1B) and thus, were predicted to have high contamination of normal cfDNA. The results reveal that, despite tumor and normal cells share constitutive genomic methylation intrinsic to metabolically living cells, cellular lineage origin, etc., there is a much greater scattering of the middle-range methylated CpGs (Supplementary Figure S1C). Consistently with this observation, comparison between tumor and normal DNA in samples of the Target cohort also showed a similar pattern with high dispersion of middle-range methylated CpGs (Supplementary Figure S1D). These results provide additional support to the very low or absent tumor DNA content in the 13 Liquidhope samples, as well as in the normal tissue samples used as controls in Target cohort. To further evaluate methylation differences within neuroblastoma subtypes and normal controls, we calculated the overall median methylation in each sample and found that there are no overall significant differences between MYCN-amplified and 11q-deleted tumors, neither in Liquidhope nor in Target cohorts (Supplementary Figure S1E and F). However, MYCN-amplified and 11q-deleted tumors got significantly hypomethylated in comparison with normal controls in both cohorts (Supplementary Figure S1E and F), indicating that global hypomethylation is prevalent across high-risk neuroblastoma types and further confirming the high content of normal cfDNA

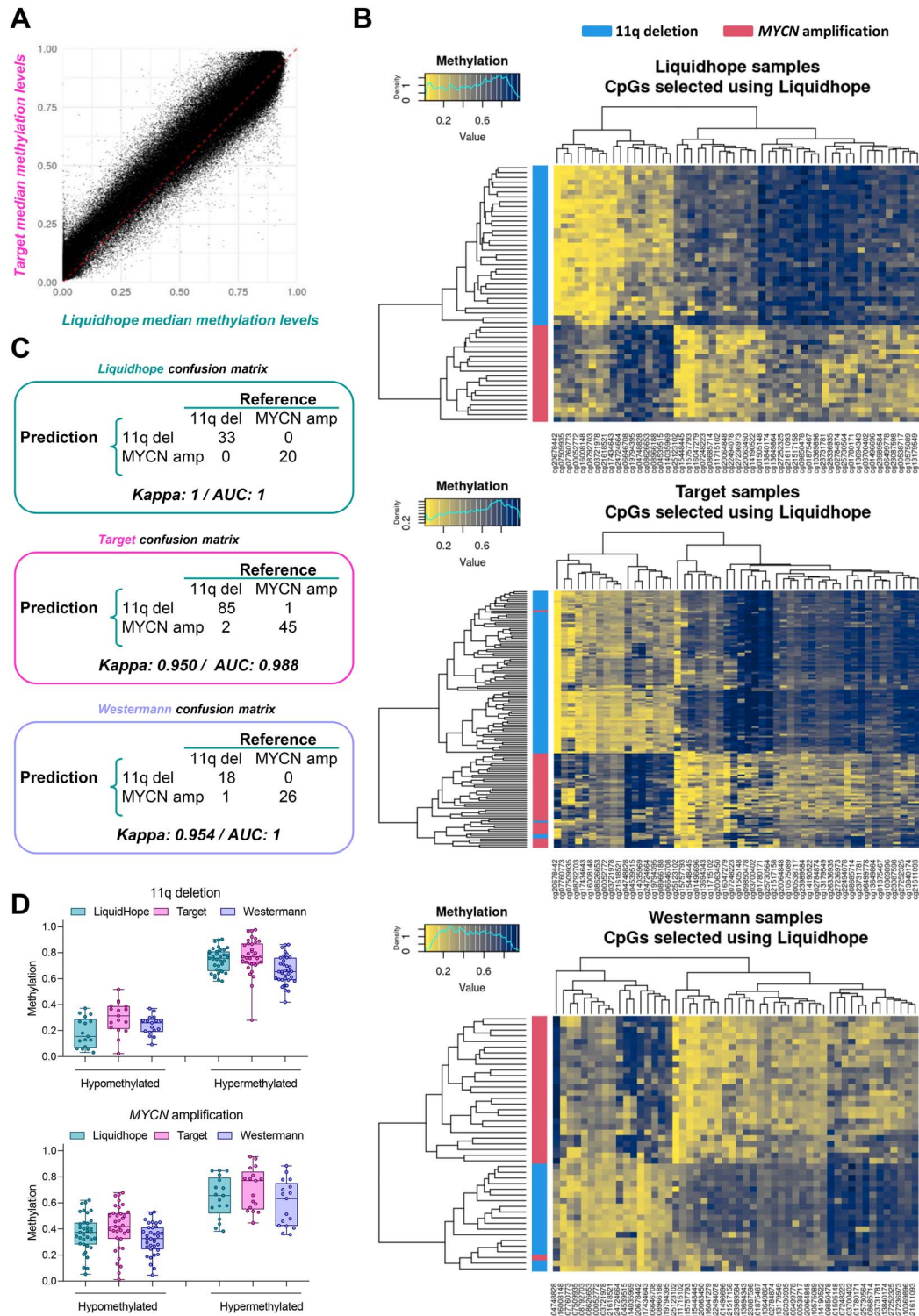


**Figure 2.** Epigenetic signature predicts 11q deletion or MYCN amplification in high-risk neuroblastomas. **(A)** Comparison between Liquidhope (X axis) and Target (Y axis) cohorts of the median methylation at each CpG (set of 235 999 common CpGs in both cohorts,  $R^2 = 0.96$ ). **(B)** Heatmap at the top panel shows the 52 CpGs (called in vertical at the bottom row) identified by elastic net regression model in Liquidhope cohort that predict 11q-deleted or MYCN-amplified neuroblastomas. Patients in the column have been ordered according to the results of the Ward hierarchical clustering algorithm. Color code for the degree of methylation is indicated at the upper left corner. The regression model was then used to predict mutation groups in the Target cohort (heatmap in the middle), and Westermann cohort (heatmap at the bottom). **(C)** Regression model-based confusion matrix is shown for each of the three cohorts, as indicated by colors, recognizing the accuracy and efficiency to predict either 11q deletion or MYCN amplification. Area under the curve (AUC) and kappa values are shown at the bottom of each corresponding cohort. **(D)** Comparison among cohorts of the methylation levels of the 52 identified CpGs, grouped by being weakly or highly methylated in 11q deletion (upper graph) or MYCN-amplified neuroblastomas (bottom graph). Color codes for each cohort are indicated at the top of each graph.

in the 13 samples that clustered together with reference DNA from white blood cells (Figure 1B).

We next generated a novel logistic regression model to predict 11q deletion or MYCN amplification in our Liquidhope cohort (Supplementary File S1). The model identified 52 CpGs that enabled a hierarchical clustering of the samples based on 11q or MYCN status (upper heatmap in Figure 2B). A confusion matrix using this same model was subsequently implemented in the Target and Westermann cohorts (central and lower heatmap in Figure 2B). In the Target cohort, the model misplaced only three samples whereas in the Westermann cohort the prediction was more accurate, only one misplaced sample (Figure 2C). Comparisons of high and low methylated CpGs in 11q-deleted and MYCN-amplified neuroblastomas across the three cohorts showed that the groups were very comparable in the methylation levels (Figure 2D). These results show the high prediction efficiency of the model, defined by the methylation levels of 52 CpGs, and support that 11q-deleted neuroblastomas share an epigenetic signature that is distinct from MYCN-amplified neuroblastomas, thus revealing divergent epigenetic pathways from origin.

### Prognostic value of eight methylated CpGs discriminating 11q/MYCN high-risk neuroblastomas

To shed light on the defective DNA methylation/demethylation pathways in the high-risk CpG signature, we first studied a detailed description of chromosomal position, affected gene or nearby genes for each signature CpG and their function (Supplementary Table S4). We next compared methylation levels at each CpGs in Liquidhope and Target cohorts, including reference cohorts containing normal cfDNA in Liquidhope and normal brain samples available in the Target cohort (Figure 3A, Supplementary Figures S2 and S3). Additionally, adrenal gland median methylation level for each CpG was included in the graph (purple dash, Figure 3A). A detailed description of chromosomal position affected gene or nearby genes for each signature CpG and their function is described in Supplementary Table S4. The prognostic value of the 52 CpGs' methylation status was evaluated, and we found 8 CpGs whose prognostic values were significant in at least one cohort and almost significant in the other (Figure 3B). Comparison with reference cohorts revealed that 11q-deleted neuroblastomas showed higher disparity than MYCN-amplified neuroblastomas in the median methylation levels for the eight CpGs named in Figure 3A. Notably, overall survival was worse for all these eight CpGs in 11q-deleted neuroblastomas with highest deviation from reference cohorts. These results demonstrate that, in addition to discriminate between 11q deletion and MYCN amplification, these eight CpGs also have prognostic value within the 11q-deleted neuroblastomas. Cg17434643 was hypomethylated in 11q-deleted neuroblastomas compared with reference cohorts (blue versus yellow) (Figure 3A) and hypomethylation had a worse prognosis in both cohorts (Figure 3B). This CpG is intergenic, near to MIR124-3, a microRNA naturally expressed in neuronal cells but downregulated in neuroblastoma cells [28]. CpG in KRT19 was hypomethylated in 11q-deleted neuroblastomas (Figure 3A) and significantly associated with worse prognosis in Liquidhope and with a trend in Target (Figure 3B). KRT19 hypomethylation in this promoter-localized CpG increased KRT19 expression in 11q-deleted neuroblastoma in Target cohort (Figure 3C). Two CpGs in KRT16 were significantly hypermethylated in 11q-deleted neuroblastomas (Figure 3A; Supplementary Figure S2A), having cg26336935 hypermethylation a significantly worse prognosis

in Target cohort (Figure 3B) and a similar trend in cg13179549 (Supplementary Figure S2B). Similar results were found in the next CpG, cg11715102, associated with worse prognosis in both cohorts (Figure 3A and B). This CpG is localized intergenic between CPXM2 and CHST15 genes (Supplementary Table S4).

Hypermethylation in cg15757793, intronic to RBFOX3, was pronounced in 11q-deleted group (Figure 3A), and associated with worse prognosis (Figure 3B). Two CpGs exonic to PEAR1 were hypermethylated in 11q-deleted neuroblastomas in comparison with normal brain and adrenal gland cohorts, but not with normal cfDNA, probably reflecting differences in cell origin (Figure 3A, Supplementary Figure S3). This hypermethylation was associated with worse prognosis in both cohorts (Figure 3B). Finally, two CpGs intronic to CCR7 (Figure 3A, Supplementary Figure S2), and a third CpG in the promoter of CSF1R (Figure 3A), showed increased hypermethylation levels in the 11q group, in comparison with normal adrenal gland and with MYCN-amplified neuroblastomas. In both cases, the hypermethylation in 11q was associated with significant worse prognosis and a trend in the second intronic CpG in CCR7 (Figure 3B, Supplementary Figure S2A and B). Other CpGs showed a trend in prognosis (Supplementary Figure S2A–D), including two CpGs within genes LMX1A and DNJC22 that were hypomethylated in MYCN-amplified (Supplementary Figure S2A–D). The remaining CpGs in the 11q/MYCN discriminating model showed defects in the DNA methylation pathways when compared to embryonal development and normal cohorts, thus revealing distinct epigenetic pathways between 11q-deleted and MYCN-amplified neuroblastomas (Supplementary Figure S3), but did not show prognostic value.

### RASSF1A hypermethylation is a common event in high-risk 11q-deleted and MYCN-amplified neuroblastomas

We next focused on RASSF1A status, a gene known to be hypermethylated in various cancer types and with proven value as a biomarker in liquid biopsy in neuroblastoma [19]. In Liquidhope, we did not observe significant differences in RASSF1A methylation levels between 11q and MYCN subgroups (Supplementary Figure S4A). Our 13 control samples containing undetectable tumor cfDNA displayed hypomethylated RASSF1A, similarly to Target controls and in contrast to 11q and MYCN tumor samples (Supplementary Figure S4A), further supporting that tumor cfDNA content in our Liquidhope controls is null or highly diluted with normal DNA. In Target cohort, we found some decrease in the methylation levels in 11q subgroup, perhaps due to the increased number of samples or their lower dispersity (Supplementary Figure S4A), but nonetheless, this difference did not render in different expression levels between 11q-deleted and MYCN-amplified subgroups (Supplementary Figure S4B). When comparing with reference cohorts, RASSF1A was markedly hypermethylated in both subgroups. To assess the methylation prognostic value of RASSF1A, we identified cg13257331 hypermethylation significantly associated with worse prognosis in 11q deletion group in Liquidhope cohort and with a trend in Target cohort (Supplementary Figure S4C). Similarly, hypermethylated cg13257331 showed a general trend toward worse prognosis in MYCN-amplified subgroup.

To elucidate if RASSF1A defect was due to overmethylation or rather a defect in demethylation at a certain time during embryogenesis, we analyzed data from available cohorts in oocytes, sperm, blastocysts (preimplant embryos) and adrenal gland. As with many other genes, RASSF1A happened to be hypermethylated in sperm and to a lesser extent in oocytes, but it is rapidly

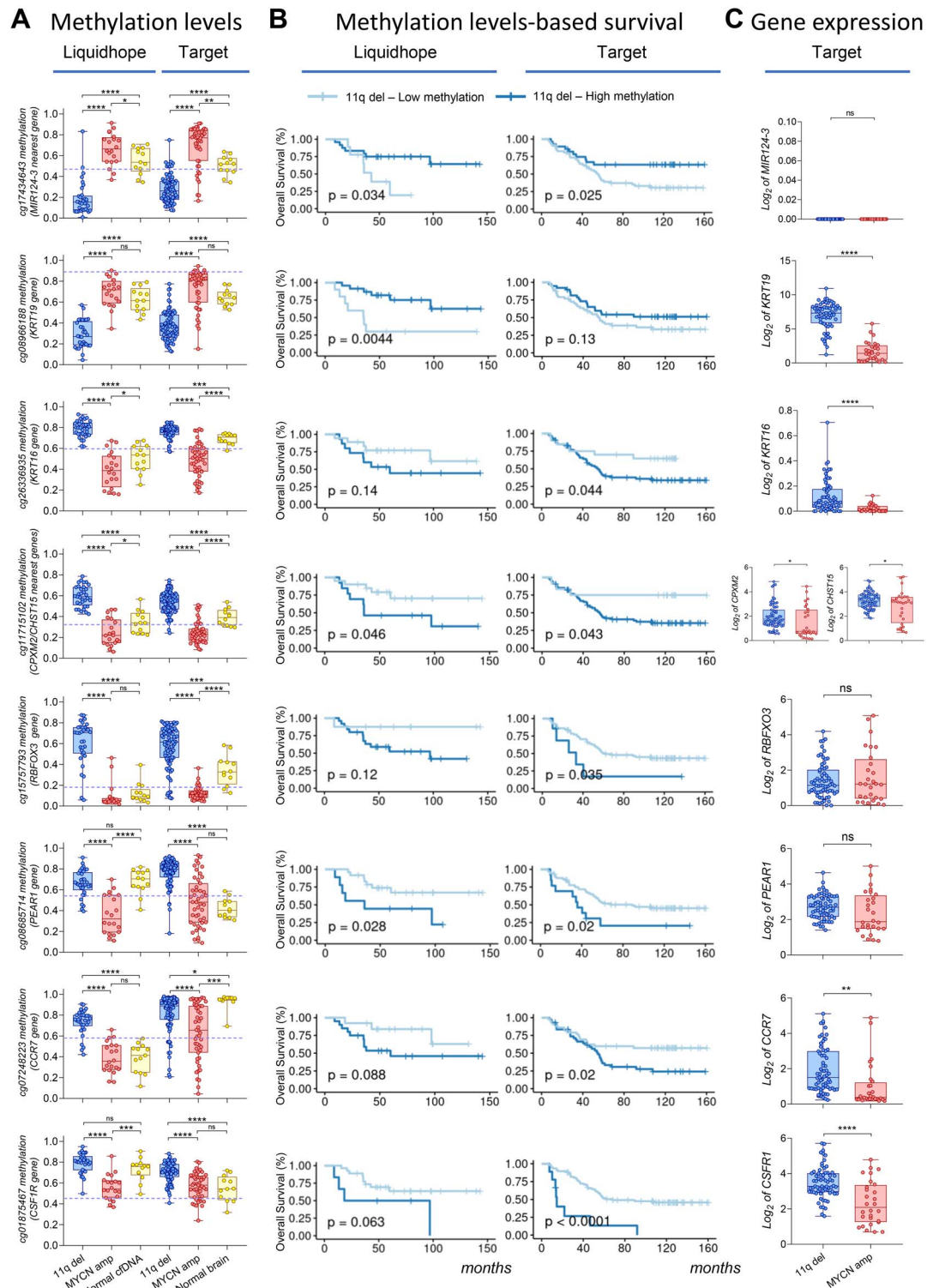


**Figure 3.** Prognostic values within 11q subgroup of eight differentially methylated CpGs between 11q-deleted and MYCN-amplified high-risk neuroblastomas identify actionable targets. **(A)** Comparison of methylation levels for each CpG between 11q-deleted (11q del, blue boxplots) and MYCN-amplified (MYCN amp, red boxplots) subgroups in Liquidhope and Target cohorts, as indicated. Reference groups are normal cfDNA and normal brain (yellow boxplots), as indicated. **(B)** Kaplan-Meier curves for overall survival in Liquidhope and Target cohorts. Samples are split in two groups according to methylation values. Threshold defining groups is chosen to maximize the evidence of survival differences between the groups (lower P-value, Wald test associated with the grouping term). **(C)** Expression levels of each CpG-associated gene were determined in paired methylation/expression samples of Target cohort, comparing 11q-deleted (blue) or MYCN-amplified (red) neuroblastomas, retrieved from R2: genomics analysis and visualization platform. Each CpG was statistically tested by paired t-test ( $P > 0.05$ , ns;  $P < 0.05$ , \*;  $P < 0.01$ , \*\*;  $P < 0.001$ , \*\*\*;  $P < 0.0001$ , \*\*\*\*).

demethylated in blastocysts (Supplementary Figure S4D). This result reveals that RASSF1A becomes hypermethylated at a later timepoint, after neural crest is formed, pointing out defects in DNA methyltransferase pathways rather than in DNA demethylases. In addition, the hypermethylation of RASSF1A in both subgroups suggests that RASSF1A hypermethylation is an early common event that occurs before epigenetic drivers imposed by MYCN amplification or by 11q deletion take place.

### Unbalanced gene expression versus methylation in 11q-deleted and MYCN-amplified high-risk neuroblastomas

To identify genes and pathways involved in the mechanisms for tumor divergence between 11q-deleted and MYCN-amplified high-risk neuroblastomas, we conducted a global differential gene expression analysis in Target cohort and depicted the percentage of significant altered genes by their chromosomal location. The highest percentage of differentially expressed genes were located in 11q followed by 17q (Figure 4A). Based in our previous studies supporting a role for deficient DNA double-strand break (DSB) repair machinery in 11q-deleted neuroblastomas, we focused our attention on genes implicated in these pathways. MYCN expression was used as an internal control of the study. Noteworthy, ATM, H2AX, CHEK1 and MRE11A, all allocated in 11q deletion, were significantly downregulated in 11q-deleted high-risk in comparison with MYCN-amplified neuroblastomas (Figure 4B). We also noted very significant downregulation in the expression of CHEK2, located in 22q. Differences in BRCA2 (13q) were also significant but subtle. All other DNA DSB repair genes did not display significant differences in their expression levels. Analysis of DNA promoter methylation showed very slight statistically significant differences, but the difference of means between 11q deletion, MYCN amplification and reference samples did never achieve 0.05 in any cohort (Figure 4C).

### Defects in DNA methylation dynamics during embryogenesis define high-risk neuroblastoma stratification

In order to understand the defective methylation processes leading to the divergent CpGs signature in the stratification of high-risk neuroblastoma, we evaluated the methylation dynamics during early embryogenesis (oocytes, sperm and blastocysts, Arima cohort) and normal adrenal gland (Figure 5A, Supplementary Figures S2D, S3C and S4D). The low methylations levels found in KRT19 during early embryogenesis contrast with the high levels found in fully developed adrenal gland, but remain low in 11q-deleted neuroblastomas (Figure 5A), suggesting a defect in KRT19 DNA methylation specific to 11q subgroup. Conversely, high methylations levels in CpGs for CPXM2/CHST15, RBFOX3, PEAR1 and CSF1R during early embryogenesis become reduced in adrenal gland but remain high in 11q deleted neuroblastomas, suggesting defects in DNA demethylases recruited at these genes. The CpG for MIR124-3 was not covered in the Arima cohort, but methylation levels in adrenal gland as well as in reference cohorts (Figure 3A) support an inversed deregulation resulting in increased DNA methylase recruitment in MYCN-amplified and increased DNA-demethylase recruitment in 11q-deleted subgroups. CpGs methylation levels for KRT16 and CCR7 increase from blastocysts to adrenal gland, but are even higher in 11q subgroup and variably lower in MYCN-amplified neuroblastomas, depending on the reference cohorts (Figures 3A and 5A). These results indicate that during the embryogenesis there are relevant deregulations in DNA

methylations and demethylation processes that are specific to 11q-deleted and to MYCN-amplified high-risk neuroblastomas.

## Discussion

Liquid biopsy stands out as a powerful source of prognostic and genetic biomarkers for subtyping and prognosis. Recent studies demonstrate the feasibility of cfDNA from liquid fluids for monitoring neuroblastoma-specific markers in very small blood volumes [29], and for determining copy number aberrations [30]. In here, we demonstrate the feasibility of liquid biopsy as a source of epigenetic biomarkers that are innate to the tumor. We identify RASSF1A methylation as a highly methylated gene in all high-risk neuroblastoma cohorts with either MYCN amplification or 11q deletion. Other cohorts studied, including blastocysts, adrenal gland, and normal brain and white cells, do not show high RASSF1 methylation levels. Thus, RASSF1A hypermethylation is a primordial event common to 11q-deleted and MYCN-amplified high-risk neuroblastomas (Figure 5B, Supplementary Figure S4). Importantly, we also identified a novel epigenetic signature for subtyping high-risk neuroblastomas. These distinct epigenetic remodeling events suggest alternative therapeutic strategies for optimal individualized treatments with drugs that have already reached clinical trials, such as transcriptional downregulation with bromodomain inhibitors or synthetic lethality with PARP inhibitors in the case of 11q-deleted neuroblastomas [8, 12–14].

The different epigenetic signature between 11q-deleted and MYCN-amplified neuroblastomas also denotes their dependency on specific cellular pathways that could be used wisely for therapeutic intervention. CpGs in the subtyping signature identify genes involved in cell signaling, in neuronal development and/or differentiation and in immune activation and cross-talk with the tumor cells (Figure 5 and Supplementary Table S4). Regarding neuronal development, three CpGs in B3GALT4, a gene coding for a key enzyme in the synthesis of gangliosides, are hypomethylated in 11q-deleted neuroblastomas, which also coincided with higher expression levels of the gene. B3GALT4, like PTPRN2, was also identified hypermethylated in stage M neuroblastomas [31]. NYAP1 regulates cellular polarity and morphology in migrating neurons [32]; thus, these observations may have implications in neuronal differentiation and differences in response to retinoic acid treatment. Several keratins were also identified by the CpGs' signature, KRT9, KRT16, KRT17, KRT32, including KRT19, whose differential methylation has already been associated with prognosis [20, 22], all with higher expression in 11q-deleted neuroblastomas (Figure 3, Supplementary Figures S2 and S3). MIR124 is naturally expressed in neuronal cells and was found downregulated in neuroblastoma cancer cells [28]. Our identified CpG is intergenic near to MIR124, but with unknown regulatory mechanism and cellular value when comparing 11q-deleted and MYCN-amplified neuroblastomas. LMX1A is a transcription factor relevant for neurogenesis and neurotransmitter phenotype [33], functioning as a suppressor of metastasis and methylation levels in the promoter have been associated with prognosis in cervix, ovarian, bladder and gastric cancers [34–37]. Similarly, we show that intronic hypomethylation in MYCN-amplified neuroblastomas is associated with worse prognosis (Supplementary Figure S2A–D).

Among CpG-targeted genes orchestrating immune activation and cross-talk with tumor cells are CCR7 and CSF1R. CCR7 is highly expressed in naïve and resting memory T cells, and is also represented in our epigenetic signature by two CpGs located in relevant regulatory elements in its intron 1



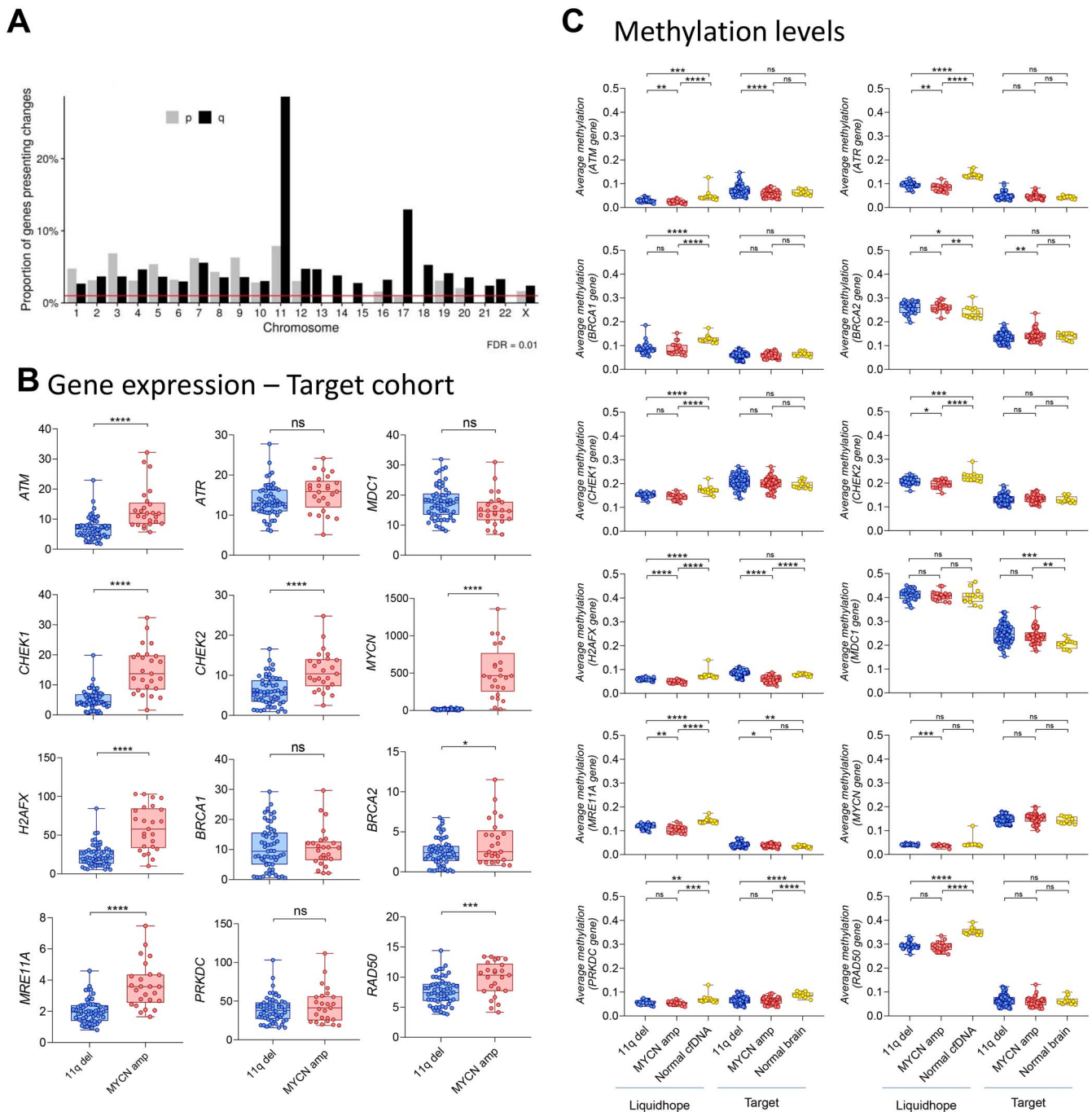


**Figure 4.** Reduced expression of DNA DSB repair genes located in 11q deletion is independent of DNA promoter methylation. **(A)** High-risk neuroblastomas in the Target cohort were selected to estimate the percentage of karyotype-based differential expression of genes with and without 11q deletion, and subsequently adjusted for *MYCN* amplification. False discovery rate (FDR) was adjusted to 0.01 and indicated with red line. **(B)** Evaluation of the principal DNA repair genes in Target cohort was evaluated in only high-risk patients, 58 patients with 11q deletion (11q del, in blue) and 25 patients with *MYCN* amplification (*MYCN* amp, in red). **(C)** Analysis of DNA methylation in the promoter region (1 kb before and after the transcription starting site) of 11q-deleted (11q del, in blue) and *MYCN*-amplified (*MYCN* amp, in red) neuroblastomas, and in reference cohorts (yellow) in Liquidhope and Target cohorts, as indicated. Each CpG was statistically tested by paired t-test ( $P > 0.05$ , ns;  $P < 0.05$ , \*;  $P < 0.01$ , \*\*;  $P < 0.001$ , \*\*\*;  $P < 0.0001$ , \*\*\*\*) comparing or between the neuroblastoma groups (blue or red), or with its reference group (yellow) in the Liquidhope and the Target cohorts.

(Figure 3, Supplementary Table S4, Supplementary Figure S2). Interestingly, both CpGs flank the transcript start site of *CCR7* transcript variant NM\_001301716, coinciding cg16047279 at a MAZ regulatory element in exon 1. Unfortunately, the Target expression cohort does not provide information to distinguish transcript variants. *CCR7* is an important factor in determining lymph node metastasis in neuroblastomas [38]. The higher

methylation and expression levels that we observed probably reveal a preferential mechanism and pathway for metastasis in 11q-deleted neuroblastomas. Thus, these two CpGs represent relevant biomarkers for stratification of high-risk tumors and in addition, may also be useful for future therapies targeting *CCR7* cross-talk with the microenvironment. The CpG in *CSF1R* promoter is yet another relevant immune target, regulating

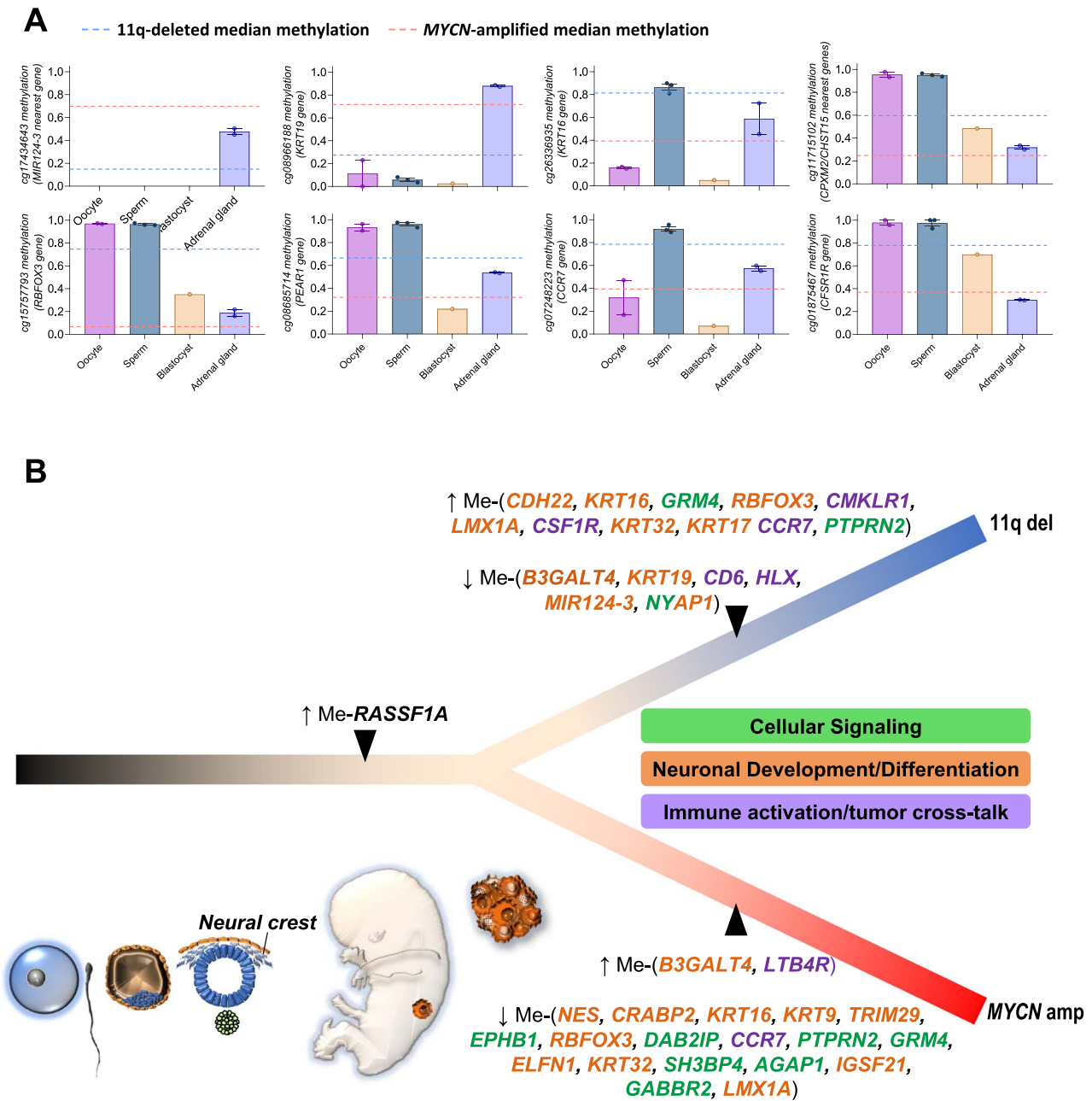


**Figure 5.** Distinct epigenetic defects in MYCN-amplified and 11q-deleted high-risk neuroblastomas identify prognostic genes as actionable targets. (A) Methylation levels of each CpG with prognostic relevance were evaluated in Arima (oocytes, sperms and blastocysts) and Lavarino cohorts (adrenal glands). Dash lines represent the median methylation levels for 11q-deleted or MYCN-amplified high-risk neuroblastomas in Liquidhope cohort. (B) Epigenetic phylogeny in high-risk neuroblastomas with either MYCN amplification (MYCN amp) or with 11q deletion (11q del) points out RASSF1A hypermethylation as an early common event in the onset of tumor evolution, and reveals divergent signatures of methylation affecting cellular signaling, neuronal differentiation and immune activation and cross-talk with tumor cells. This epigenetic signature supports high-risk neuroblastomas with either 11q deletion or MYCN amplification as independent tumor entities that evolved through different chromatin remodeling pathways.

tumor-macrophage crosstalk, with higher methylation levels in 11q-deleted neuroblastomas and also increased expression levels in this subgroup (Figure 3A and C). Inhibition of CSF1R in animal models increased chemotherapeutic efficacy, suggesting its potential benefit in patients who have limited anti-tumor T-cell responses [39]. Our results support that high-risk 11q-deleted neuroblastomas may as well benefit from CSF1R modulators. The CpG in CMKLR1 is located in a proximal enhancer-like signature and is also hypermethylated in 11q-deleted neuroblastomas, with increased expression levels in this subgroup (Supplementary Table S4, Supplementary Figure S3).

Interestingly, CMKLR1 expression was shown as a prognostic factor and possible therapeutic target in neuroblastoma [40]. It is important to note that some of these genes could be expressed under pathological conditions in tumor cells, like CSF1R, relevant in low claudin expression breast tumors, mediating a switch from the proliferative to the invasive state [41]. However, the presence of differentially methylated CpGs in genes thought to be uniquely expressed in the immune system (i.e. CD6, CTLR4 and HLX) suggests that liquid biopsy may also contain a valuable representation of what it is happening in the tumor microenvironment.

Altogether, we demonstrate the feasibility of very low quantities of bloodstream circulating DNA and provide new tools for convenient comparisons with external cohorts, independent of the different technical approaches employed. We provide for the first time a new script to stratify high-risk neuroblastomas based on the methylation on 52 CpGs, no matter the source of tumor DNA, the unmethylated cysteines conversion technique or the DNA methylation analysis (sequencing versus arrays). This new tool is provided in [Supplementary File S1](#). We also identify two divergent epigenetic pathways for 11q-deleted and MYCN-amplified neuroblastomas that support their common origin but different evolution. Therefore, 11q-deleted and MYCN-amplified neuroblastomas constitute two independent tumor entities with distinct cellular deregulated processes, mostly focused on cell signaling, neuronal differentiation and immune activity, based on the differentially affected CpGs. Moreover, 11q-deletion neuroblastomas display significant reduced levels of DNA DSB repair genes allocated in 11q, further supporting a role for combined haploinsufficiency of these genes in the progression of the disease and the use of PARP inhibitor to treat this tumor subtype. Expression differences found in genes involved in DNA DSB repair are not due to their promoter methylation, but possibly to gene dosage or alternatively to other epigenetic modifications such as histone acetylations and methylations. Our results represent a significant advance as we can now use this novel epigenetic signature in high-risk neuroblastomas as a source of biomarkers, some with potential prognostic and therapeutic value, and strengthens liquid biopsy for disease stratification and follow-up.

#### Key Points

- Development of a method for overcoming very low-input cfDNA for whole-methylome profiling by enzymatic EM-seq.
- Bioinformatics model for subtype and highly accurate prognosis prediction of outcome in high-risk neuroblastoma.
- Identification of epigenomic changes that serve as actionable targets for treatment of pediatric patients.
- Validation of the feasibility of using blood-derived cfDNA for precision medicine approach.

#### Authors' contributions

The authors confirm contribution to the paper as follows: conception and design: E.M.T., S.H. and J.F.M. Financial support: J.F.M. Collection and assembly of data: E.M.T. Provision of study materials or patients: A.C. and V.C. Data analysis and interpretation: E.M.T., E.V.E.C., A.E.-C., M.G., S.H. and J.F.M. Manuscript writing: all authors.

#### Data availability

Liquidhope cohort data is deposited at Geo database with Series accession number GSE221317 (<https://www.ncbi.nlm.nih.gov/geo/query/acc.cgi?acc=GSE221317>).

#### Supplementary Data

Supplementary data are available online at <https://academic.oup.com/bib>.

#### Acknowledgements

We are grateful to D. Ramal (Pediatric Oncology Clinical Trials Unit, University Hospital La Fe) for update and support on patients' data analyzed in [Supplementary Table S1](#).

#### Funding

TRANSCAN-2 consortium LIQUIDHOPE by Fundación Científica de la Asociación Española Contra el Cáncer (TRNSC18001FON); Spanish Ministry of Science and Innovation (MICINN, PID2020-119323RB-I00 grant); 'Sumemos muchas manos por los niños enfermos' non-profit organization; Instituto de Salud Carlos III (ISCIII), Spain and 'European Social Fund Plus (ESF+)' of the European Union (Miguel Servet Program, CP20/00179, ISCIII-MICINN to E.V.); Fundación Científica de la Asociación Española Contra el Cáncer (PRDVA19004CORO to E.C.).

#### References

1. Heitzer E, Haque IS, Roberts CES, et al. Current and future perspectives of liquid biopsies in genomics-driven oncology. *Nat Rev Genet* 2019;**20**:71–88.
2. Gu H, Smith ZD, Bock C, et al. Preparation of reduced representation bisulfite sequencing libraries for genome-scale DNA methylation profiling. *Nat Protoc* 2011;**6**:468–81.
3. Ladenstein R, Potschger U, Valteau-Couanet D, et al. Investigation of the role of dinutuximab beta-based immunotherapy in the SIOPEN high-risk neuroblastoma 1 trial (HR-NBL1). *Cancers (Basel)* 2020;**12**:309.
4. Maris JM. Recent advances in neuroblastoma. *N Engl J Med* 2010;**362**:2202–11.
5. Ackermann S, Cartolano M, Hero B, et al. A mechanistic classification of clinical phenotypes in neuroblastoma. *Science* 2018;**362**:1165–70.
6. Brodeur GM, Seeger RC, Schwab M, et al. Amplification of N-myc in untreated human neuroblastomas correlates with advanced disease stage. *Science* 1984;**224**:1121–4.
7. Peifer M, Hertwig F, Roels F, et al. Telomerase activation by genomic rearrangements in high-risk neuroblastoma. *Nature* 2015;**526**:700–4.
8. Sanmartin E, Munoz L, Piqueras M, et al. Deletion of 11q in neuroblastomas drives sensitivity to PARP inhibition. *Clin Cancer Res* 2017;**23**:6875–87.
9. Coronado E, Yanez Y, Vidal E, et al. Intratumoral immunosuppression profiles in 11q-deleted neuroblastomas provide new potential therapeutic targets. *Mol Oncol* 2021;**15**:364–80.
10. Irwin MS, Naranjo A, Zhang FF, et al. Revised neuroblastoma risk classification system: a report from the Children's Oncology Group. *J Clin Oncol* 2021;**39**:3229–41.
11. Schleiermacher G, Janoueix-Lerosey I, Ribeiro A, et al. Accumulation of segmental alterations determines progression in neuroblastoma. *J Clin Oncol* 2010;**28**:3122–30.
12. Henssen A, Althoff K, Odersky A, et al. Targeting MYCN-driven transcription by BET-bromodomain inhibition. *Clin Cancer Res* 2016;**22**:2470–81.
13. Iniguez AB, Alexe G, Wang EJ, et al. Resistance to epigenetic-targeted therapy engenders tumor cell vulnerabilities associated with enhancer remodeling. *Cancer Cell* 2018;**34**:922–938.e7.
14. Puissant A, Frumm SM, Alexe G, et al. Targeting MYCN in neuroblastoma by BET bromodomain inhibition. *Cancer Discov* 2013;**3**:308–23.
15. Alaminos M, Davalos V, Cheung NK, et al. Clustering of gene hypermethylation associated with clinical risk groups in neuroblastoma. *J Natl Cancer Inst* 2004;**96**:1208–19.

16. Teitz T, Wei T, Valentine MB, et al. Caspase 8 is deleted or silenced preferentially in childhood neuroblastomas with amplification of MYCN. *Nat Med* 2000;**6**:529–35.
17. van Noesel MM, van Bezouw S, Salomons GS, et al. Tumor-specific down-regulation of the tumor necrosis factor-related apoptosis-inducing ligand decoy receptors DcR1 and DcR2 is associated with dense promoter hypermethylation. *Cancer Res* 2002;**62**:2157–61.
18. Yang Q, Zage P, Kagan D, et al. Association of epigenetic inactivation of RASSF1A with poor outcome in human neuroblastoma. *Clin Cancer Res* 2004;**10**:8493–500.
19. van Zogchel LMJ, Lak NSM, Verhagen O, et al. Novel circulating hypermethylated RASSF1A ddPCR for liquid biopsies in patients with pediatric solid tumors. *JCO Precis Oncol* 2021;**5**:1738–48.
20. Caren H, Djos A, Nethander M, et al. Identification of epigenetically regulated genes that predict patient outcome in neuroblastoma. *BMC Cancer* 2011;**11**:66.
21. Decock A, Ongenaert M, Cannoodt R, et al. Methyl-CpG-binding domain sequencing reveals a prognostic methylation signature in neuroblastoma. *Oncotarget* 2016;**7**:1960–72.
22. Decock A, Ongenaert M, Hoebeeck J, et al. Genome-wide promoter methylation analysis in neuroblastoma identifies prognostic methylation biomarkers. *Genome Biol* 2012;**13**:R95.
23. Merkel A, Fernandez-Callejo M, Casals E, et al. gemBS: high throughput processing for DNA methylation data from bisulfite sequencing. *Bioinformatics* 2019;**35**:737–42.
24. Jiang P, Chan CW, Chan KC, et al. Lengthening and shortening of plasma DNA in hepatocellular carcinoma patients. *Proc Natl Acad Sci U S A* 2015;**112**:E1317–25.
25. Okae H, Chiba H, Hiura H, et al. Genome-wide analysis of DNA methylation dynamics during early human development. *PLoS Genet* 2014;**10**:e1004868.
26. Gomez S, Castellano G, Mayol G, et al. DNA methylation fingerprint of neuroblastoma reveals new biological and clinical insights. *Epigenomics* 2015;**7**:1137–53.
27. Schuyler RP, Merkel A, Raineri E, et al. Distinct trends of DNA methylation patterning in the innate and adaptive immune systems. *Cell Rep* 2016;**17**:2101–11.
28. Sharif S, Ghahremani MH, Soleimani M. Induction of morphological and functional differentiation of human neuroblastoma cells by miR-124. *J Biosci* 2017;**42**:555–63.
29. Lodrini M, Wunschel J, Thole-Kliesch TM, et al. Circulating cell-free DNA assessment in biofluids from children with neuroblastoma demonstrates feasibility and potential for minimally invasive molecular diagnostics. *Cancers (Basel)* 2022;**14**:2080.
30. Van Paemel R, Vandeputte C, Raman L, et al. The feasibility of using liquid biopsies as a complementary assay for copy number aberration profiling in routinely collected paediatric cancer patient samples. *Eur J Cancer* 2022;**160**:12–23.
31. Olsson M, Beck S, Kogner P, et al. Genome-wide methylation profiling identifies novel methylated genes in neuroblastoma tumors. *Epigenetics* 2016;**11**:74–84.
32. Wang S, Li X, Zhang Q, et al. Nyap1 regulates multipolar-bipolar transition and morphology of migrating neurons by Fyn phosphorylation during corticogenesis. *Cereb Cortex* 2020;**30**:929–41.
33. Chung S, Kim CH, Kim KS. Lmx1a regulates dopamine transporter gene expression during ES cell differentiation and mouse embryonic development. *J Neurochem* 2012;**122**:244–50.
34. Dong W, Feng L, Xie Y, et al. Hypermethylation-mediated reduction of LMX1A expression in gastric cancer. *Cancer Sci* 2011;**102**:361–6.
35. Lai HC, Lin YW, Huang TH, et al. Identification of novel DNA methylation markers in cervical cancer. *Int J Cancer* 2008;**123**:161–7.
36. Su HY, Lai HC, Lin YW, et al. An epigenetic marker panel for screening and prognostic prediction of ovarian cancer. *Int J Cancer* 2009;**124**:387–93.
37. Zhao Y, Guo S, Sun J, et al. Methylcap-seq reveals novel DNA methylation markers for the diagnosis and recurrence prediction of bladder cancer in a Chinese population. *PLoS One* 2012;**7**:e35175.
38. Zhang L, Yeger H, Das B, et al. Tissue microenvironment modulates CXCR4 expression and tumor metastasis in neuroblastoma. *Neoplasia* 2007;**9**:36–46.
39. Webb MW, Sun J, Sheard MA, et al. Colony stimulating factor 1 receptor blockade improves the efficacy of chemotherapy against human neuroblastoma in the absence of T lymphocytes. *Int J Cancer* 2018;**143**:1483–93.
40. Tummeler C, Snapkov I, Wickstrom M, et al. Inhibition of chemerin/CMKLR1 axis in neuroblastoma cells reduces clonogenicity and cell viability in vitro and impairs tumor growth in vivo. *Oncotarget* 2017;**8**:95135–51.
41. Patsialou A, Wang Y, Pignatelli J, et al. Autocrine CSF1R signaling mediates switching between invasion and proliferation downstream of TGFbeta in claudin-low breast tumor cells. *Oncogene* 2015;**34**:2721–31.